

Phase structure and electrochemical properties of $\text{La}_{0.7}\text{Ce}_{0.3}\text{Ni}_{3.75}\text{Mn}_{0.35}\text{Al}_{0.15}\text{Cu}_{0.75-x}\text{Fe}_x$ hydrogen storage alloys

LIU Bao-zhong^{1,2}, LI An-ming¹, FAN Yan-ping¹, HU Meng-juan¹, ZHANG Bao-qing¹

1. School of Materials Science and Engineering, Henan Polytechnic University, Jiaozuo 454000, China;
2. State Key Laboratory of Metastable Materials Science and Technology, Yanshan University, Qinhuangdao 066004, China

Received 20 August 2012; accepted 25 September 2012

Abstract: $\text{La}_{0.7}\text{Ce}_{0.3}\text{Ni}_{3.75}\text{Mn}_{0.35}\text{Al}_{0.15}\text{Cu}_{0.75-x}\text{Fe}_x$ ($x=0-0.20$) hydrogen storage alloys were synthesized by induction melting and subsequent annealing treatment, and phase structure and electrochemical characteristics were investigated. All alloys consist of a single LaNi_5 phase with CaCu_5 structure, and the lattice constant a and the cell volume (V) of the LaNi_5 phase increase with increasing x value. The maximum discharge capacity gradually decreases from 319.0 mA·h/g ($x=0$) to 291.9 mA·h/g ($x=0.20$) with the increase in x value. The high-rate dischargeability at the discharge current density of 1200 mA/g decreases monotonically from 53.1% ($x=0$) to 44.2% ($x=0.20$). The cycling stability increases with increasing x from 0 to 0.20, which is mainly ascribed to the improvement of the pulverization resistance.

Key words: hydrogen storage alloy; AB_5 -type hydrogen storage alloys; phase structures; electrochemical property; kinetics; Ni-MH battery; LaNi_5 phase

1 Introduction

AB_5 -type hydrogen storage alloys have attracted much attention due to their widespread applications in rechargeable nickel/metal hydride (Ni/MH) batteries [1–3]. However, wide application of Ni/MH battery is hindered due to the high cost of negative electrode materials. In order to decrease the raw cost, lots of Co-less or Co-free alloys were prepared by substituting Co with foreign metals, such as, Fe, Cu, Si, whose raw cost has been much lower than that of Co [4–6]. The Co-free alloy with high Cu content was developed and commercially used [7]. However, the electrochemical performance, especially cycling stability, is not satisfactory. Thus, it is necessary to improve the electrochemical properties and further reduce the raw cost.

For AB_5 type alloys, it is believed that partial substitution of Fe for Ni or Co does not change the

original CaCu_5 structure, and plays an important role in improving the cycling stability and other electrochemical properties [8,9]. VIVET et al [10] studied the electrochemical hydrogen storage properties of $\text{MmNi}_{4.07}\text{Mn}_{0.63}\text{Al}_{0.2}\text{Co}_{0.4-x}\text{Fe}_x$ ($0 \leq x \leq 0.4$) alloys and found that Fe-containing alloy electrodes behave as well as Co-containing electrodes in terms of cycle life with a slight capacity reduction. WEI et al [11] investigated the substitution of Fe for Ni in $\text{LaNi}_{4.05-x}\text{Al}_{0.45}\text{Mn}_{0.5}\text{Fe}_x$ ($0 \leq x \leq 0.5$) alloys and found that the cycle stability increased with the increase of x value and the high-rate dischargeability of the alloys increased with increasing x value from 0 to 0.5. Moreover, SAKAI et al [12] investigated the hydrogen storage properties of $\text{Mm}(\text{NiCoMnAlX})_5$ alloys and found that the value of $\Delta V/V$ was 10.4% for the alloy $X=\text{Fe}$ and lower than 16% for the alloy $X=\text{Cu}$. It is shown that Fe is more efficient than Cu in reducing the volume swelling of hydride. Consequently, it is expected that the substitution of Cu by cheaper Fe can improve the electrochemical property

Foundation item: Project (51001043) supported by the National Natural Science Foundation of China; Project (NCET2011) supported by Program for New Century Excellent Talents in University, China; Project (201104390) supported by China Postdoctoral Science Special Foundation; Project (20100470990) supported by China Postdoctoral Science Foundation; Project (2012IRTSTHN007) supported by Program for Innovative Research Team (in Science and Technology) in the University of Henan Province, China; Project (2011J1003) supported by Baotou Science and Technology Project, China; Project (B2010-13) supported by the Doctoral Foundation of Henan Polytechnic University, China

Corresponding author: LIU Bao-zhong; Tel/Fax: +86-391-3989859; E-mail: bzliu@hpu.edu.cn
DOI: 10.1016/S1003-6326(11)61525-2

without increasing the alloy cost.

In this work, on the basis of the merits of Co-free alloy and the belief that the Fe substitution may result in some noticeable modification of the alloys, phase structure and electrochemical properties of $\text{La}_{0.7}\text{Ce}_{0.3}\text{Ni}_{3.75}\text{Mn}_{0.35}\text{Al}_{0.15}\text{Cu}_{0.75-x}\text{Fe}_x$ ($x=0-0.20$) alloys were investigated systematically.

2 Experimental

$\text{La}_{0.7}\text{Ce}_{0.3}\text{Ni}_{3.75}\text{Mn}_{0.35}\text{Al}_{0.15}\text{Cu}_{0.75-x}\text{Fe}_x$ ($x=0-0.20$) alloys were synthesized by induction melting of the metal elements (La, Ce, Ni, Mn, Al, Cu: 99.9% purity) under argon atmosphere and then were annealed at 1223 K for 10 h.

The phases of the alloy powders were determined by X-ray diffraction (XRD) using a Rigaku D/max 2500PC powder diffractometer with $\text{Cu K}\alpha$ radiation. The phase structures of alloys were analyzed using Jade-5 software. Scanning electron microscopy (SEM) images were obtained with HITACHI-4800 scanning electron microscope.

All the alloy electrodes for test were prepared by cold pressing the mixture of 0.15 g alloy powders of 0.038–0.075 μm and 0.75 g nickel carbonyl powders into a pellet of 10 mm in diameter under 15 MPa. Electrochemical measurements were performed at 298 K in a standard tri-electrode system, consisting of a working electrode (metal hydride), a counter electrode ($\text{Ni}(\text{OH})_2/\text{NiOOH}$), and a reference electrode (Hg/HgO) with 6 mol/L KOH solution as electrolyte. Each electrode was charged for 7 h at 60 mA/g and discharged to -0.6 V versus Hg/HgO at 60 mA/g at 298 K. After every charging/discharging, the rest time was 10 min. In evaluating the high-rate dischargeability, discharge capacity values of the alloy electrodes at different discharge current densities were measured. The high-rate dischargeability HRD was defined as $(C_d/C_{\text{max}}) \times 100\%$, where C_d was the discharge capacity at the discharge current density J_d ($J_d=60, 300, 600, 900$ and 1200 mA/g, respectively), and C_{max} was the maximum discharge capacity at the discharge current density of 60 mA/g.

The linear polarization curve and potential-step measurement were obtained on an electrochemical working station (PARSTAT 2273). Linear polarization curve was obtained by scanning the electrodes from -5 to 5 mV (vs open circuit potential). For potential-step measurement, the electrodes in fully charged state were discharged with potential step of 0.5 V for 3600 s.

3 Results and discussion

3.1 Phase structure

Figure 1 shows XRD patterns of $\text{La}_{0.7}\text{Ce}_{0.3}\text{Ni}_{3.75}$ -

$\text{Mn}_{0.35}\text{Al}_{0.15}\text{Cu}_{0.75-x}\text{Fe}_x$ alloys. It is found that all alloys are identified with CaCu_5 type hexagonal structure with $P6/mmm$ space group. Calculated lattice parameters of the alloys are listed in Table 1. It can be seen that the lattice constant a and the cell volume V of LaNi_5 phase increase with increasing x value, which is ascribed to the larger atomic radius of Fe (1.72 Å) than that of Cu (1.57 Å). The FWHM (full widths at half-maximum) of (1 1 1) peak of the alloys is also listed in Table 1. It is observed that the FWHM decreases with the increase of Fe content, indicating that the alloy homogeneity increases and/or the internal strain decreases [13].

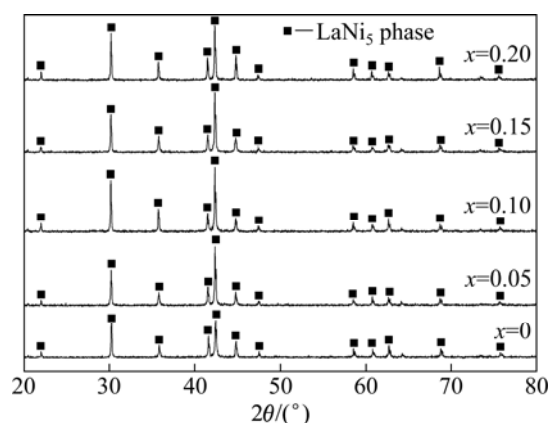


Fig. 1 XRD patterns of $\text{La}_{0.7}\text{Ce}_{0.3}\text{Ni}_{3.75}\text{Mn}_{0.35}\text{Al}_{0.15}\text{Cu}_{0.75-x}\text{Fe}_x$ alloys

Table 1 Lattice parameters of $\text{La}_{0.7}\text{Ce}_{0.3}\text{Ni}_{3.75}\text{Mn}_{0.35}\text{Al}_{0.15}\text{Cu}_{0.75-x}\text{Fe}_x$ alloys

x	$a/\text{Å}$	$c/\text{Å}$	$V/\text{Å}^3$	FWHM/(°)
0.00	5.0198	4.0464	88.3049	0.139
0.05	5.0220	4.0470	88.3954	0.123
0.10	5.0242	4.0483	88.5013	0.120
0.15	5.0250	4.0492	88.5491	0.118
0.20	5.0300	4.0439	88.6093	0.117

3.2 Activation performance and maximum discharge capability

The cycle number needed to be activated (N_a) and the maximum discharge capacity (C_{max}) of $\text{La}_{0.7}\text{Ce}_{0.3}\text{Ni}_{3.75}\text{Mn}_{0.35}\text{Al}_{0.15}\text{Cu}_{0.75-x}\text{Fe}_x$ alloy electrodes are given in Table 2. The N_a decreases from 4 to 2 with increasing x value, indicating that the substitution of Fe for Cu facilitates the activation property of alloy electrodes. Generally, decisive factors of the activation capability of the alloy are the surface characteristic and interstitial dimension [14]. ZHANG et al [15] reported that the oxidation film on the alloy surface increased the additive internal energy, which led to the poorer activation performance. Due to the lower surface energy of Fe, the increase of Fe makes the surface oxide layer become thick, which degrades the activation property. Fortunately,

GUO et al [16] pointed out that the larger unit cell volume resulted in the larger interstitial hole size for hydrogen atoms to occupy, which led to the smaller strain energy that hydrogen atoms go in and out the crystal. The V of LaNi_5 phase increases with increasing x value, and then strain energy decreases, which is favorable for the activation performance of the alloys. Therefore, it is reasonable to believe that the V of LaNi_5 phase is more important for the activation property in the present work. The C_{\max} of $\text{La}_{0.7}\text{Ce}_{0.3}\text{Ni}_{3.75}\text{Mn}_{0.35}\text{Al}_{0.15}\text{Cu}_{0.75-x}\text{Fe}_x$ alloy electrodes decreases from 319.0 mA·h/g ($x=0$) to 291.9 mA·h/g ($x=0.20$). In general, the maximum discharge capacity is related to the crystalline structure and electrochemical kinetics. BRATENG et al [17] pointed out that the larger the cell volume is, the higher the discharge capacity is. The increase in the V of LaNi_5 phase is favorable for the discharge capacity. On the contrary, the oxidation on the alloy surface will decrease the activity site on the alloy surface and degrade the charge-transfer reaction on the alloy surface, which leads to a loss in the discharge capacity. Moreover, the increase of Fe and decrease of Cu with increasing x value will decrease the activity site due to the increase of the surface oxide, which makes hydrogen diffuse from inner of the bulky electrode to the surface more difficultly, which is detriment to the hydrogen diffusion. Thus, the degradation of electrochemical kinetics is prominent for the decrease of the C_{\max} of $\text{La}_{0.7}\text{Ce}_{0.3}\text{Ni}_{3.75}\text{Mn}_{0.35}\text{Al}_{0.15}\text{Cu}_{0.75-x}\text{Fe}_x$ alloy electrodes in the present work.

Table 2 Electrochemical properties of $\text{La}_{0.7}\text{Ce}_{0.3}\text{Ni}_{3.75}\text{Mn}_{0.35}\text{Al}_{0.15}\text{Cu}_{0.75-x}\text{Fe}_x$ alloys electrodes

x	$C_{\max}/(\text{mA}\cdot\text{h}\cdot\text{g}^{-1})$	N_a	HRD ₁₂₀₀ ^a /%	$S_{100}/\%$
0.00	319.0	4	53.1	73.3
0.05	314.6	3	52.0	77.0
0.10	312.3	2	50.5	79.6
0.15	309.1	2	46.7	82.6
0.20	291.9	2	44.2	85.6

^a The high-rate dischargeability at the discharge current density of 1200 mA/g.

3.3 High-rate dischargeability and electrochemical kinetics

Figure 2 shows the relationship between the HRD and the discharge current density of the $\text{La}_{0.7}\text{Ce}_{0.3}\text{Ni}_{3.75}\text{Mn}_{0.35}\text{Al}_{0.15}\text{Cu}_{0.75-x}\text{Fe}_x$ alloy electrodes. The HRD of the alloy electrodes decreases with increasing x value. The HRD at the discharge current density of 1200 mA/g (HRD₁₂₀₀) is listed in Table 2. It can be seen that HRD₁₂₀₀ decreases monotonically from 53.1% ($x=0$) to 44.2% ($x=0.20$).

It is well known that the HRD is dominated by the electrochemical kinetics of charge-transfer reaction at the

electrode/electrolyte interface and the hydrogen diffusion rate within the bulky alloy electrode, which is mainly determined by the charge-transfer resistance on the surface, the exchange current density (J_0) and the hydrogen diffusion coefficient (D) [18].

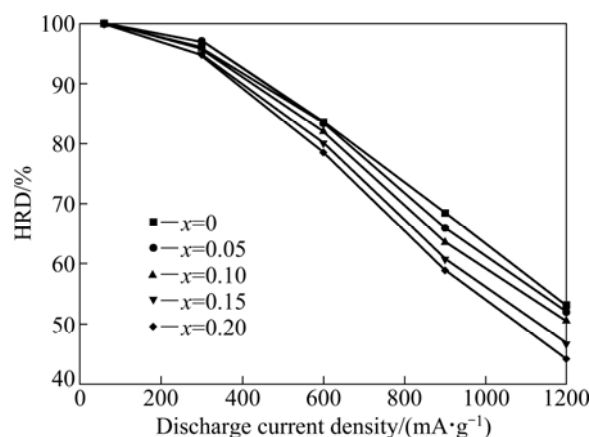


Fig. 2 High rate dischargeability (HRD) of $\text{La}_{0.7}\text{Ce}_{0.3}\text{Ni}_{3.75}\text{Mn}_{0.35}\text{Al}_{0.15}\text{Cu}_{0.75-x}\text{Fe}_x$ alloy electrodes

Figure 3 shows the linear polarization curves of $\text{La}_{0.7}\text{Ce}_{0.3}\text{Ni}_{3.75}\text{Mn}_{0.35}\text{Al}_{0.15}\text{Cu}_{0.75-x}\text{Fe}_x$ alloy electrodes at 50% depth of discharge (DOD) and 298 K. The polarization resistances (R_p) are calculated through estimating the slopes of linear polarization curves, and listed in Table 3. The R_p values of the alloy electrodes increase from 187.6 mΩ·g ($x=0$) to 299.5 mΩ·g ($x=0.20$), which implies that the polarization increases with the increase of Fe content. Furthermore, the J_0 can also describe the charge-transfer process. The J_0 value can be calculated according to the following formula [19].

$$J_0 = RT / (FR_p) \quad (1)$$

where R , T , F and R_p are the mole gas constant, the thermodynamic temperature, the Faraday constant and the polarization resistance, respectively. The J_0 values

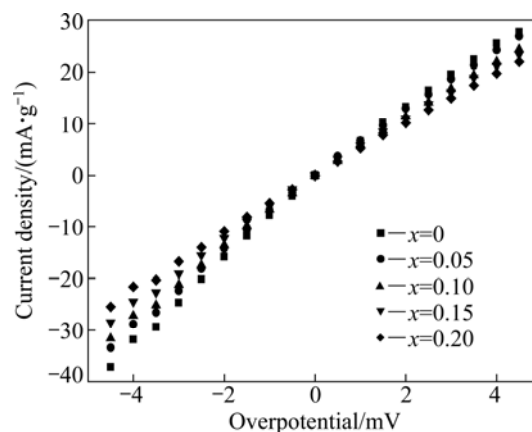


Fig. 3 Linear polarization curves of $\text{La}_{0.7}\text{Ce}_{0.3}\text{Ni}_{3.75}\text{Mn}_{0.35}\text{Al}_{0.15}\text{Cu}_{0.75-x}\text{Fe}_x$ alloy electrodes at 50% DOD at 298 K

are calculated by Eq. (1) and listed in Table 3. It is clear that the J_0 decreases from 137.8 mA/g ($x=0$) to 86.3 mA/g ($x=0.20$). As mentioned above, the increase of x value will lead to the increase of surface oxide, which degrades the electrocatalytic activity on the alloy surface. Thus, the increase of the R_p and the decrease of the J_0 should be ascribed to the formation of the oxidation on the alloy surface.

Table 3 Electrochemical kinetic characteristics of $\text{La}_{0.7}\text{Ce}_{0.3}\text{Ni}_{3.75}\text{Mn}_{0.35}\text{Al}_{0.15}\text{Cu}_{0.75-x}\text{Fe}_x$ alloys electrodes

x	$R_p/(\text{m}\Omega\cdot\text{g})$	$J_0/(\text{mA}\cdot\text{g}^{-1})$	$D/(10^{-11}\text{ cm}^2\cdot\text{s}^{-1})$
0	187.6	137.8	7.76
0.05	208.1	124.2	7.67
0.10	231.8	111.5	7.44
0.15	258.2	100.1	7.20
0.20	299.5	86.3	7.06

The diffusion coefficient of hydrogen in the alloy electrodes is determined by the potential-step method. Figure 4 shows the semi-logarithmic plots of the anodic current vs the time response of $\text{La}_{0.7}\text{Ce}_{0.3}\text{Ni}_{3.75}\text{Mn}_{0.35}\text{Al}_{0.15}\text{Cu}_{0.75-x}\text{Fe}_x$ alloy electrodes. ZHENG et al [20] reported that in a large anodic potential-step test, after a long discharge time, the diffusion current varies with time according to the following equation:

$$\lg J = \lg \left(\frac{6FD}{\rho a^2} (c_0 - c_s) \right) - \frac{\pi^2}{2.303} \frac{D}{r^2} t \quad (2)$$

where J is anodic current density; D is the hydrogen diffusion coefficient; ρ is the mass density of the alloy; r is the radius of the alloy particle; c_0 is the initial hydrogen concentration in the bulk of the alloy; c_s is the surface hydrogen concentration of the alloy; t is the discharge time.

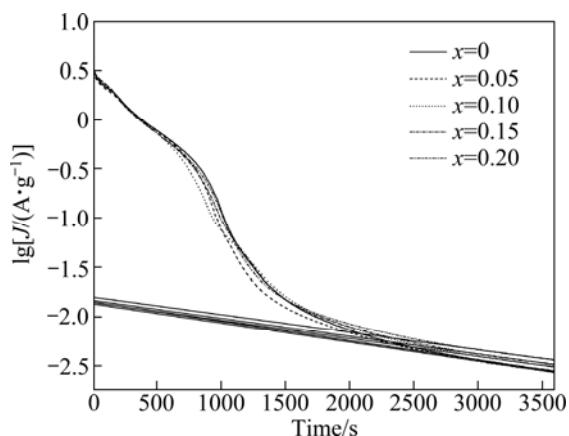


Fig. 4 Semi-logarithmic plots of anodic current vs time responses of $\text{La}_{0.7}\text{Ce}_{0.3}\text{Ni}_{3.75}\text{Mn}_{0.35}\text{Al}_{0.15}\text{Cu}_{0.75-x}\text{Fe}_x$ alloy electrodes

Assuming that the alloy has a similar particle distribution with an average particle radius of 13 μm according to previous study [21], D is calculated and summarized in Table 3. The D values of the $\text{La}_{0.7}\text{Ce}_{0.3}\text{Ni}_{3.75}\text{Mn}_{0.35}\text{Al}_{0.15}\text{Cu}_{0.75-x}\text{Fe}_x$ alloy electrodes decrease from 7.76×10^{-11} ($x=0$) to 7.06×10^{-10} cm^2/s ($x=0.20$). This implies that the hydrogen diffusivity in the alloys decreases with increasing x value. IWAKURA et al [22] reported that the increase of the cell volume led to the increase of hydride stability and resulted in the decrease of hydrogen diffusion in the bulky alloy. The V of LaNi_5 phase increases with increasing x value, which leads to the decrease of the hydrogen diffusion. Moreover, as mentioned above, the increase of x value makes the hydrogen diffuse from the bulk of the alloys to the surface more difficultly, which is unfavorable to the hydrogen diffusion property. Thus, the D value of the $\text{La}_{0.7}\text{Ce}_{0.3}\text{Ni}_{3.75}\text{Mn}_{0.35}\text{Al}_{0.15}\text{Cu}_{0.75-x}\text{Fe}_x$ alloy electrodes decreases with increasing the x value.

3.4 Cycling stability

The cycle stability is an extremely important factor for the service life of hydrogen storage alloys. The cycling capacity retention rate is expressed as $S_n = C_n/C_{\max} \times 100\%$, where C_n is the discharge capacity at the n th cycle. The cycling capacity retention of the alloy electrode as a function of cycle number is shown in Fig. 5. The cycling stability increases with increasing x from 0 to 0.20. The cycling capacity retention rate after 100 charge/discharge cycles (S_{100}) is listed in Table 2. It can be seen that S_{100} increases from 73.3% ($x=0$) to 85.6% ($x=0.20$).

It is confirmed that the fundamental reasons for the capacity decay of the electrode alloy are the pulverization and oxidation of the alloy during charge-discharge cycle [23]. The improvement of the cycling stability of the alloy electrodes may be ascribed to the following factors. Figure 6 shows the SEM images of

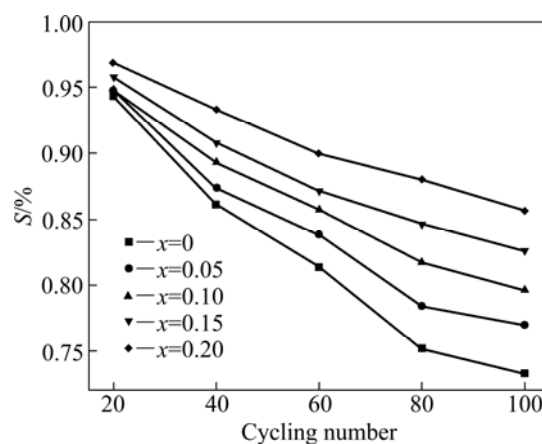


Fig. 5 Cycling capacity retention of $\text{La}_{0.7}\text{Ce}_{0.3}\text{Ni}_{3.75}\text{Mn}_{0.35}\text{Al}_{0.15}\text{Cu}_{0.75-x}\text{Fe}_x$ alloy electrode as function of cycle number

$\text{La}_{0.7}\text{Ce}_{0.3}\text{Ni}_{3.75}\text{Mn}_{0.35}\text{Al}_{0.15}\text{Cu}_{0.75-x}\text{Fe}_x$ alloys after 100 cycles. It can be seen that the particle size of alloy is 3–4 μm when x is 0. The particle size of alloy with $x=5$ is larger compared with the alloy with $x=0$, indicating that the addition of Fe can decrease the pulverization of alloy. Moreover, as mentioned above, the V of LaNi_5 phase increases, which lowers the strain energy when hydrogen atoms go in and out the crystal, and therefore contributes to the pulverization resistance of the alloy electrode. In addition, the alloys with good homogeneity and/or small internal strain possessed good anti-pulverization [24]. From the analysis of FWHM for the XRD peak of LaNi_5 phase, the homogeneity of the alloys enhances and/or the internal strain becomes lower with increasing x value, which contributes to the higher cycling stability. Thus, the substitution of Fe for Cu can improve the cycling stability of the alloy electrodes.

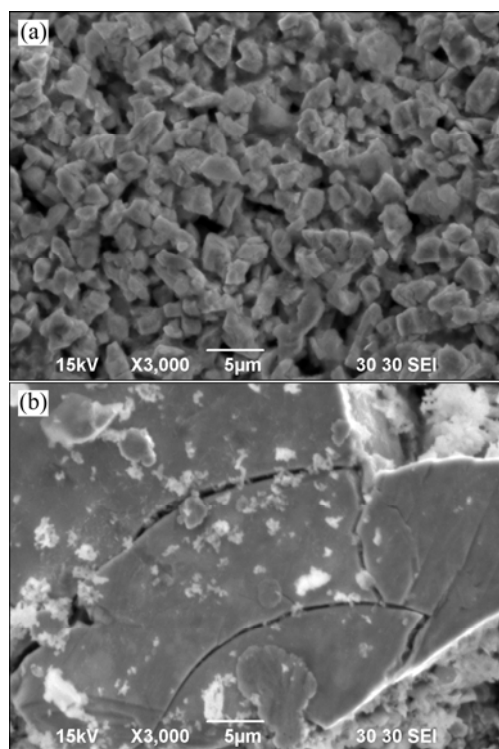


Fig. 6 SEM images of $\text{La}_{0.7}\text{Ce}_{0.3}\text{Ni}_{3.75}\text{Mn}_{0.35}\text{Al}_{0.15}\text{Cu}_{0.75-x}\text{Fe}_x$ alloys after 100 cycles: (a) $x=0$; (b) $x=0.20$

4 Conclusions

1) All of the alloys have LaNi_5 phase disclosed by XRD pattern. As the Fe content increases in the alloys, the lattice constant a and the cell volume V of LaNi_5 phase increase.

2) The maximum discharge capacity monotonously decreases from 319.0 $\text{mA}\cdot\text{h/g}$ ($x=0$) to 291.9 $\text{mA}\cdot\text{h/g}$ ($x=0.20$).

3) The HRD of the alloy electrodes decreases with increasing x value, and the charge-transfer reaction at the

electrode/electrolyte interface and the hydrogen diffusion of alloy electrodes are responsible for the high-rate dischargeability.

4) S_{100} increases from 73.3% ($x=0$) to 85.6% ($x=0.20$), which mainly results from improvement of the pulverization resistance of the alloy electrodes.

References

- [1] LI Y, HAN S, LI J, ZHU X, HU L. Study on kinetics and electrochemical properties of $\text{Ml}_{0.70}\text{Mg}_{0.30}(\text{Ni}_{3.95}\text{Co}_{0.75}\text{Mn}_{0.15}\text{Al}_{0.15})_x$ ($x=0.60, 0.64, 0.68, 0.70, 0.76$) alloys [J]. *Mater Chem Phys*, 2008, 108: 92–96.
- [2] YE H., HUANG Y X, CHEN J X, ZHANG H. $\text{MmNi}_{3.55}\text{Co}_{0.75}\text{Mn}_{0.4}\text{Al}_{0.3}\text{B}_{0.3}$ hydrogen storage alloys for high-power nickel/metal hydride batteries [J]. *J Power Sources*, 2002, 103: 293–299.
- [3] QIAN C X, CHEN L Y, RONG H, YUAN X M. Hydrogen production by mixed culture of several facultative bacteria and anaerobic bacteria [J]. *Progress in Natural Science: Materials International*, 2011, 21: 506–511.
- [4] LI P, HOU Z H, YANG T, SHANG H W, QU X H, ZHANG Y H. Structure and electrochemical hydrogen storage characteristics of as-cast and annealed $\text{La}_{0.8-x}\text{Sm}_x\text{Mg}_{0.2}\text{Ni}_{3.15}\text{Co}_{0.2}\text{Al}_{0.1}\text{Si}_{0.05}$ ($x=0-0.4$) alloys [J]. *J Rare Earth*, 2012, 30: 696–700.
- [5] YANG S Q, HAN S M, SONG J Z, LI Y. Influences of molybdenum substitution for cobalt on the phase structure and electrochemical kinetic properties of AB-type hydrogen storage alloys [J]. *J Rare Earth*, 2011, 29: 692–697.
- [6] WU F, ZHANG M, MU D. Effect of B and Fe substitution on structure of AB_3 -type Co-free hydrogen storage alloy [J]. *Transactions of Nonferrous Metals Society of China*, 2010, 20: 1885–1891.
- [7] WANG Y J, YUAN H T, WANG G S, ZHANG Y S. Characteristics of novel Co-free $\text{MlNi}_{4.2-x}\text{Cu}_{0.5}\text{Al}_{0.3}\text{Zn}_x$ ($0 < x < 0.1$) hydrogen storage alloys [J]. *Solid State Ionics*, 2002, 148: 509–512.
- [8] TANG W Z, GAI Y X, ZHENG H Y. Deterioration of copper-containing mischmetal-nickel-based hydrogen absorption electrode materials [J]. *J Alloys Compd*, 1995, 224: 292–298.
- [9] LI S L, WANG P, CHEN W, LUO G, CHEN D M, YANG K. Hydrogen storage properties of $\text{LaNi}_{3.8}\text{Al}_{1.0}\text{M}_{0.2}$ ($\text{M}=\text{Ni, Cu, Fe, Al, Cr, Mn}$) alloys [J]. *J Alloys Compd*, 2009, 485: 867–871.
- [10] VIVET S, JOUBERT J M, KNOSP B, PERCHERON-GUÉGAN A. Effects of cobalt replacement by nickel, manganese, aluminium and iron on the crystallographic and electrochemical properties of AB_5 -type alloys [J]. *J Alloys Compd*, 2003, 356–357: 779–783.
- [11] WEI X D, LIU S S, DONG H, ZHANG P, LIU Y N, ZHU J W, YU G. Microstructures and electrochemical properties of Co-free AB_5 -type hydrogen storage alloys through substitution of Ni by Fe [J]. *Electrochim Acta*, 2007, 52: 2423–2428.
- [12] SAKAI T, HAZAMA T, MIYAMURA H, KURIYAMA N. Rare-earth-based alloy electrodes for a nickel-metal hydride battery [J]. *J Less-Common Met*, 1991, 172–174: 1175–1184.
- [13] BRATENG R, GULBRANDSEN-DAHL S, VAØEN L O, SOLBERG J K, TUNOLD R. Structural and electrochemical characterization of a melt spun AB_5 -type alloy [J]. *J Alloys Compd*, 2005, 396: 100–107.
- [14] ZHOU Y, LEI Y Q, LUO Y C, CHENG S A, WANG Q D. Activation of hydrogen-storage electrode alloy $\text{Ml}(\text{Ni, Co, Mn, Ti})_5$ produced by gas atomization [J]. *Acta Metallurgica Sinica*, 1996, 32: 857–881.
- [15] ZHANG P, WANG X, TU J, VHEN G. Effect of surface treatment

- on the structure and high-rate dischargeability properties of AB₅-type hydrogen storage alloy [J]. *J Rare Earth*, 2009, 27(3): 510–513.
- [16] GUO J H, CHEN D M, YU J, ZHANG J H, LIU G Z, YANG K. Study on high rate discharge performance and mechanism of AB₅ type hydrogen storage alloys [J]. *J Rare Earths*, 2004, 22: 509–603.
- [17] BRATENG R, GULBRANDSEN-DAHL S, VAØEN L O, SOLBERG J K, TUNOLD R. Structural and electrochemical characterization of a melt spun AB₅-type alloy [J]. *J Alloys Compd*, 2005, 396: 100–107.
- [18] ZHANG Q Q, SU G, LI A S, LIU K Y. Electrochemical performance of AB₅-type hydrogen storage alloy modified with Co₃O₄ [J]. *Transactions of Nonferrous Metals Society of China*, 2011, 21: 1428–1434.
- [19] NOTTEN P, HOKKELING P. Double-phase hydride forming compounds: a new class of highly electrocatalytic materials [J]. *J Electrochem Soc*, 1991, 138: 1877–1885.
- [20] ZHENG G, POPOV B N, WHITE R E. Electrochemical determination of the diffusion coefficient of hydrogen through an LaNi_{4.25}Al_{0.75} electrode in alkaline aqueous solution [J]. *J Electrochem Soc*, 1995, 142: 2695–2698.
- [21] LIU B, FAN G, WANG Y, MI G, WU Y, WANG L. Crystallographic and electrochemical characteristics of melt-spun Ti–Zr–Ni–Y alloys [J]. *Int J Hydrogen Energy*, 2008, 33: 5801–5805.
- [22] IWAKURA C, FUKUDA K, SENOH H, INOUE H, MATSUOKA M, YAMAMOTO Y. Effects of substitution with foreign metals on the crystallographic, thermodynamic and electrochemical properties of AB₅-type hydrogen storage alloys [J]. *Electrochim Acta*, 1996, 41: 117–121.
- [23] CHARTOUNI D, MELI F, ZUTTEL A, GROSS K, SCHLAPBACH L. The influence of cobalt on the electrochemical cycling stability of LaNi₅-based hydride forming alloys [J]. *J Alloys Compd*, 1996, 241(1–2): 160–166.
- [24] YE H, ZHANG H, CHENG J X, HUANG T S. Effect of Ni content on the structure, thermodynamic and electrochemical properties of the non-stoichiometric hydrogen storage alloys [J]. *J Alloys Compd*, 2000, 308: 163–171.

La_{0.7}Ce_{0.3}Ni_{3.75}Mn_{0.35}Al_{0.15}Cu_{0.75-x}Fe_x 合金的相结构和电化学储氢性能

刘宝忠^{1,2}, 李安铭¹, 范燕平¹, 胡梦娟¹, 张宝庆¹

1. 河南理工大学 材料科学与工程学院, 焦作 454000;

2. 燕山大学 亚稳材料制备技术与科学国家重点实验室, 秦皇岛 066004

摘要: 采用感应熔炼和热处理的方法制备 La_{0.7}Ce_{0.3}Ni_{3.75}Mn_{0.35}Al_{0.15}Cu_{0.75-x}Fe_x($x=0\sim 0.20$) 合金, 并研究合金的相结构和电化学储氢性能。全部合金均为单一的具有 CaCu₅ 结构的 LaNi₅ 相, LaNi₅ 相的晶格常数 a 和晶胞体积随着 x 值的增加而增大。最大放电容量随着 x 值的增加从 319.0 mA·h/g($x=0$)降低到 291.9 mA·h/g($x=0.20$)。在 1200 mA/g 的电流密度下 HRD 值从 53.1%($x=0$)降低到 44.2%($x=0.20$)。合金电极的循环稳定性随着 x 值的增加而增强, 这主要归因于合金抗粉化能力的增强。

关键词: 储氢合金; AB₅ 型储氢合金; 相结构; 电化学性能; 动力学; 镍氢电池; LaNi₅ 相

(Edited by YANG Hua)